Electrochemical Materials and Technologies

ARTICLE

Electrochemical Materials and Technologies

eISSN: 2949-0561

Cite this: Electrochem. Mater. Technol. 4 (2025) 20254047

$Ln_2NiO_{4+\delta}$-based oxygen electrodes for proton-conducting $Sr_{0.98}Zr_{0.95}Yb_{0.05}O_{3-\delta}$ electrolyte for application in IT-SOFCs

Anastasia Meshcherskikh [a]*, Adelya Khaliullina [a], Elena Pikalova [a], Liliya Dunyushkina [a]

Received: 1 November 2024
Accepted: 6 December 2024
Published online: 9 January 2025

DOI: 10.15826/elmattech.2025.4.047

Layered lanthanide nickelates $Ln_2NiO_{4+\delta}$ are considered as potential cathode materials in solid oxide fuel cells. In this study, the chemical stability, thermal expansion and electrical conductivity of a number of layered nickelates, namely $La_2NiO_{4+\delta}$, $Pr_{1.7}Sr_{0.3}NiO_{4+\delta}$, $Pr_{1.7}Ca_{0.3}NiO_{4+\delta}$ and $Nd_{1.9}Ca_{0.1}NiO_{4+\delta}$, are investigated. Based on the chemical stability, thermal expansion and electrical conductivity studies, the composite material consisting of $Pr_{1.7}Ca_{0.3}NiO_{4+\delta}$ and $Sr_{0.98}Zr_{0.95}Yb_{0.05}O_{3-\delta}$ oxides (PCN-SZYb) was selected as a suitable oxygen electrode for the proton-conducting $Sr_{0.98}Zr_{0.95}Yb_{0.05}O_{3-\delta}$ electrolyte. The electrochemical behavior of the electrolyte-supported cells with the symmetrical porous PCN-SZYb electrodes was investigated in air with different humidities in the temperature range of 350–800 °C. The impregnation of a porous electrode backbone with the praseodymium nitrate solution enhanced the activity of the electrodes by approximately 3 times. The electrochemical behavior of the composite electrode in contact with the $Sr_{0.98}Zr_{0.95}Yb_{0.05}O_{3-\delta}$ electrolyte is consistent with the literature data on the $Ln_2NiO_{4+\delta}$-based electrodes and related proton-conducting electrolytes.

keywords: layered nickelates, proton-conducting electrolyte, SOFC, polarization resistance, electrochemical activity, praseodymium nitrate impregnation

1. Introduction

Due to the growing energy need and aggravation of environmental problems associated mainly with CO_2 emissions from the combustion of fossil fuels, electrochemical electricity generation using solid oxide fuel cells (SOFC) has been attracting significant attention in recent decades. SOFCs convert the chemical energy of fuel into electricity with high efficiency and minimal emissions of pollutants into the atmosphere [1, 2]. The SOFCs based on proton-conducting electrolytes operate at lower temperatures and have higher efficiency compared to the SOFCs based on oxygen-ion electrolytes [3–5]. Perovskite structured materials based on strontium zirconate are promising proton-conducting electrolytes due to their high thermal and chemical stability, appreciable ionic conductivity, and low electronic conductivity. The substitution of zirconium with acceptor cations, as well as a small strontium deficiency, contribute to an increase in the ionic conductivity [6–14]. We recently studied the phase composition, microstructure and electrical properties of $Sr_xZr_{0.95}Yb_{0.05}O_{3-\delta}$ ($x = 0.94$–1.00) series [13, 14]. It was found that the ionic conductivity and the hydration ability reach a maximum at $x = 0.98$, which was explained by an increase in the concentration of oxygen vacancies to maintain electroneutrality. Therefore, $Sr_{0.98}Zr_{0.95}Yb_{0.05}O_{3-\delta}$ was recommended as a promising electrolyte material.

The search for relevant electrode materials is an important task in the field of development of efficient SOFCs. SOFC cathodes must meet the following basic requirements: (1) mixed electronic and ionic conductivity in oxidizing atmospheres, (2) high catalytic activity to oxygen dissociation and reduction, (3) thermal expansion coefficient similar to that of an electrolyte; (3) chemical stability in contact with the electrolyte material in the fabrication and operation conditions; (4) reasonable cost [15, 16]. In the last decades, layered nickelates with the generic formula $Ln_2NiO_{4+\delta}$ (Ln = La, Pr, Nd) have attracted considerable interest for potential

a: Institute of High-Temperature Electrochemistry of the Ural Branch of the Russian Academy of Sciences, Ekaterinburg 620066, Russia

* Corresponding author: lazyty@mail.ru

application as cathodes for SOFCs operating at intermediate temperatures (IT-SOFCs) [17–41]. The crystalline structure of these materials is alternating layers of perovskite LnNiO$_3$ and rock salt LnO. $Pr_2NiO_{4+\delta}$-based materials were reported to serve as effective electrodes in symmetrical reversible protonic ceramic cells with the Ba(Ce,Zr)O$_3$-based electrolyte [29–32]. Modified La_2NiO_4 [33–35] and Nd_2NiO_4 [36] were also found to be suitable cathodes in the fuel cells with the proton-conducting Ba(Ce,Zr)O$_3$ electrolyte. Nevertheless, only a limited number of studies on the use of $Ln_2NiO_{4+\delta}$-based electrodes in contact with other proton-conducting electrolytes have been reported [37–40].

Based on the above considerations, the present research aims to study the applicability of the $Ln_2NiO_{4+\delta}$-based layered nickelates as oxygen electrodes for the $Sr_{0.98}Zr_{0.95}Yb_{0.05}O_{3-\delta}$ (SZYb) electrolyte. $La_2NiO_{4+\delta}$ (LN), $Pr_{1.7}Sr_{0.3}NiO_{4+\delta}$ (PSN), $Pr_{1.7}Ca_{0.3}NiO_{4+\delta}$ (PCN), and $Nd_{1.9}Ca_{0.1}NiO_{4+\delta}$ (NCN) were considered as potential electrode materials. The phase composition, thermal expansion, electrical conductivity of the nickelates and their chemical stability in contact with the SZYb electrolyte at elevated temperatures were studied. To improve the thermal and chemical compatibility of the electrode and electrolyte materials, the composite electrodes $Ln_2NiO_{4+\delta}$-SZYb were prepared, and their electrical conductivity was studied. Based on the results obtained, the most suitable oxygen electrode for application in contact with the SZYb electrolyte in IT-SOFCs was selected, and its electrochemical behavior was examined. The effect of the impregnation of a porous electrode backbone with the praseodymium nitrate solution on the electrochemical activity was investigated.

2. Experimental

2.1. Preparation of samples

SZYb was synthesized by the solution combustion method using $ZrO(NO_3)_2 \cdot 2H_2O$, $Yb(NO_3)_3 \cdot nH_2O$ and $SrCO_3$ (all > 99 % purity) as precursors. $ZrO(NO_3)_2 \cdot 2H_2O$ and $Yb(NO_3)_3 \cdot nH_2O$ were dissolved in distilled water and ethanol, respectively. These solutions were mixed and $SrCO_3$ powder was added in the required ratio. Then citric acid and glycine were added as a complexant and a fuel, respectively, so that the molar ratio of metal cations, glycine, and citric acid was 2 : 2 : 1. The resulting suspension was slowly heated on a hotplate while stirring, until strontium carbonate was completely dissolved, which occurred due to the presence of nitrate ions formed during the dissolution of zirconium and ytterbium nitrates. Then, the mixture was heated without stirring until it ignited. The resulting grayish beige powder was ground and calcined at 1200 °C for 2 h to enable the formation of a crystalline perovskite phase. For the fabrication of ceramic SZYb samples, the calcined material was thoroughly ground, uniaxially pressed into pellets under a pressure of 130 MPa, and sintered at 1600 °C for 5 h. The relative densities of the sintered pellets were calculated as a ratio of a geometric density, which was determined as a ratio of the sample weight to its volume, to X-ray density. The density of the sintered pellets was about 95 % of the X-ray density.

The powders of LN, PSN, PCN, and NCN were synthesized by a solid state reaction method from La_2O_3 (99.99 % purity), Nd_2O_3 (99.99 % purity), $Pr_2(CO_3)_3 \cdot 6H_2O$ (99.9 % purity), $SrCO_3$ (99 % purity), $Ca(NO_3)_2 \cdot 4H_2O$ (99.97 %), $Ni(NO_3)_2 \cdot 6H_2O$ (99.97 %) starting reagents. The precursors were combined in a given ratio, activated in a planetary mill for 1 hour with the addition of isopropyl alcohol, dried and synthesized at 1150 °C, 10 h and 1250 °C for 5 h with the intermediate ballmilling for 1 h. The final powders were milled for 1 h.

To study the chemical stability of the electrolyte and electrode materials in contact with each other at high temperatures, the powders of SZYb and $Ln_2NiO_{4+\delta}$-based oxide were mixed in a weight ratio of 1 : 1, uniaxially pressed into pellets and calcined at temperatures of 1200–1400 °C for 5 h. To find out whether the chemical interaction of oxides occurs or not, the phase composition of the calcined mixtures was investigated using the XRD method.

For the electrical and thermomechanical studies, the bar-shaped ceramic samples from the nickelate powders with the linear dimensions of 5 × 4 × 25 mm were prepared by uniaxial pressing with a butyral resin binder at 6 MPa with following sintering at 1450 °C for 5 h. The relative density of the samples was in the range of 87–97 %. To measure the electrical conductivity of $Ln_2NiO_{4+\delta}$-SZYb composite materials, the powders of the corresponding nickelate and SZYb were mixed in a weight ratio of 1 : 1, pressed into rectangular bars and sintered at 1300 °C for 4 h. The resulting composite ceramics had the dimensions of 1.0 × 0.25 × 0.15 cm^3 and the relative density of 75–80 %.

Based on the obtained results on the thermal expansion, electrical conductivity and chemical stability of $Ln_2NiO_{4+\delta}$-based materials, $Pr_{1.7}Ca_{0.3}NiO_{4+\delta}$ was selected as the electronconducting phase for the composite electrode. To study the electrochemical properties of PCN-SZYb electrodes, three symmetrical

electrolyte-supported button cells PCN-SZYb | SZYb | PCN-SZYb were prepared. The composite electrodes were made by mixing the powders of SZYb and $Pr_{1.7}Ca_{0.3}NiO_{4+\delta}$ in a weight ratio of 1 : 1 in ethanol, drying and mixing with polyvinyl butyral as a binder; the obtained ink was painted symmetrically on the opposite faces of SZYb pellets and sintered at 1100 °C for 2 h. The thickness of SZYb pellets and the electrode area were 0.134 cm and 0.18 cm^2, respectively. It should be noted that the impregnation of a porous electrode backbone with the praseodymium nitrate solution followed by calcination to produce PrO_x nanoparticles distributed inside the porous electrode is widely used to activate the oxygen electrode [41, 42]. To identify the impact of PrO_x addition on the electrochemical properties of the PCN-based oxygen electrode, one of the prepared button cells was left in its original state (Cell 1), while in the two other cells the porous PCN-SZYb electrodes were impregnated with the solution of praseodymium nitrate in ethanol (13 g · L^{-1}) and calcined at 900 °C for 1 h to increase the activity of the electrode to the oxygen reduction reaction. In Cell 2, each of two electrodes was impregnated with 0.14 mL · cm^{-2} of solution (1.8 mg Pr_6O_{11} cm^{-2}), while 0.28 mL · cm^{-2} of solution (3.6 mg Pr_6O_{11} cm^{-2}) was added to each electrode in Cell 3.

2.2. Characterization of samples

The phase composition of the prepared powders of $Ln_2NiO_{4+\delta}$-based oxides, SZYb, and the composite materials $Ln_2NiO_{4+\delta}$-SZYb, calcined at different temperatures, were characterized by the X-ray diffraction (XRD) method on a D/MAX-2200 Rigaku (Japan) diffractometer using monochromatic CuKα radiation (λ = 1.5418 Å) at room temperature. The diffraction patterns were recorded in the range of 2θ from 15 ° to 90 ° with a step of 0.02 °. Analysis of the phase composition and calculation of the crystallographic parameters were carried out using the software package MDI Jade 6.5 and database PDF-2 ICDD.

The specific surface area of the $Ln_2NiO_{4+\delta}$-based powders was defined using a BET method by means of a SORBI N.4.1 analyzer. The microstructures of composite electrodes and ceramic electrolyte were examined using scanning electron microscopy (SEM) supplemented with the energy dispersive X-ray spectroscopy (EDX) using the MIRA 3 LMU (Tescan, Czech Republic) and the INCA Energy 350 X-Max 80 equipment (Oxford Instruments, USA). The cross-sectional fracture surface of a button cell was studied.

The thermal expansion of the bar-shaped samples of $Ln_2NiO_{4+\delta}$ was measured under the heating mode (2 °C · min^{-1}) in a temperature range of 100–900 °C in air by the dilatometric method using a DIL 402 C Netzsch GmbH dilatometer. The thermal expansion coefficient (TEC) was determined from the slope of the dependence of $\Delta L/L_0$ (L_0 – the sample length at 100 °C, ΔL – the length change upon heating) on temperature.

The electrical conductivity of the $Ln_2NiO_{4+\delta}$ bars was measured in the temperature range of 300–900 °C in a cooling mode (5 °C · min^{-1}) in air using the four-probe DC method. The measured conductivities were corrected to zero porosity using the following equation as described, for example, in [43]:

$$\sigma_d = \sigma_p \frac{1+p/2}{(1-\rho)^{2/3}}, \quad (1)$$

where p is the porosity and σ_d and σ_p are the conductivities of the dense and porous samples, respectively.

The measurement of electrical conductivity of the composite samples $Ln_2NiO_{4+\delta}$-SZYb was carried out in the air with different humidities (pH_2O = 0.04; 0.61 and 3.3 kPa) in the temperature range of 250–900 °C. The current electrodes were made by painting Pt paste on the ends of the bars and sintering at 1000 °C for 2 h, while the potential probes for measuring a voltage drop were prepared by winding two Pt wires around the bars. The electrochemical performance of the button cells with the supporting SZYb electrolyte and PCN-SZYb electrodes was investigated by the impedance spectroscopy and cyclic voltammetry methods using potentiostat-galvanostat Elins P–45X (Electrochemical instruments, Russia). Impedance spectra were recorded in the frequency range of $5 \cdot 10^5$–10^{-2} Hz with an amplitude of 30 mV. The current-voltage dependencies were measured at a scan rate of 1 mV · sec^{-1} in the range of –0.1–0.1 V. The measurements were carried out in the temperature range of 350–800 °C. Both DC and AC electrical measurements were carried out in dry and humid atmospheres. The dry atmosphere was obtained by blowing the atmospheric air through a column filled with zeolite beads. The residual water vapor partial pressure was equal to 0.04 kPa (measured by Baikal-3M hygrometer (JSC Etalon, Russia)). The humid air was obtained by pumping the atmospheric air through a bubbler with thermostatically controlled water (at 0 °C, pH_2O = 0.61 kPa, and at 26 °C, pH_2O = 3.3 kPa).

3. Results

3.1. Phase composition and morphology of samples

The XRD patterns of the SZYb and $Ln_2NiO_{4+\delta}$ powders presented in Figures 1a–e indicate that all

synthesized oxides are single phase and have the same structures as the parent materials. SZYb has an orthorhombic perovskite structure (*Pnma* space group) with the unit cell parameters: $a = 5.8190(1)$ Å, $b = 5.8190(1)$ Å, $c = 5.7946(2)$ Å.

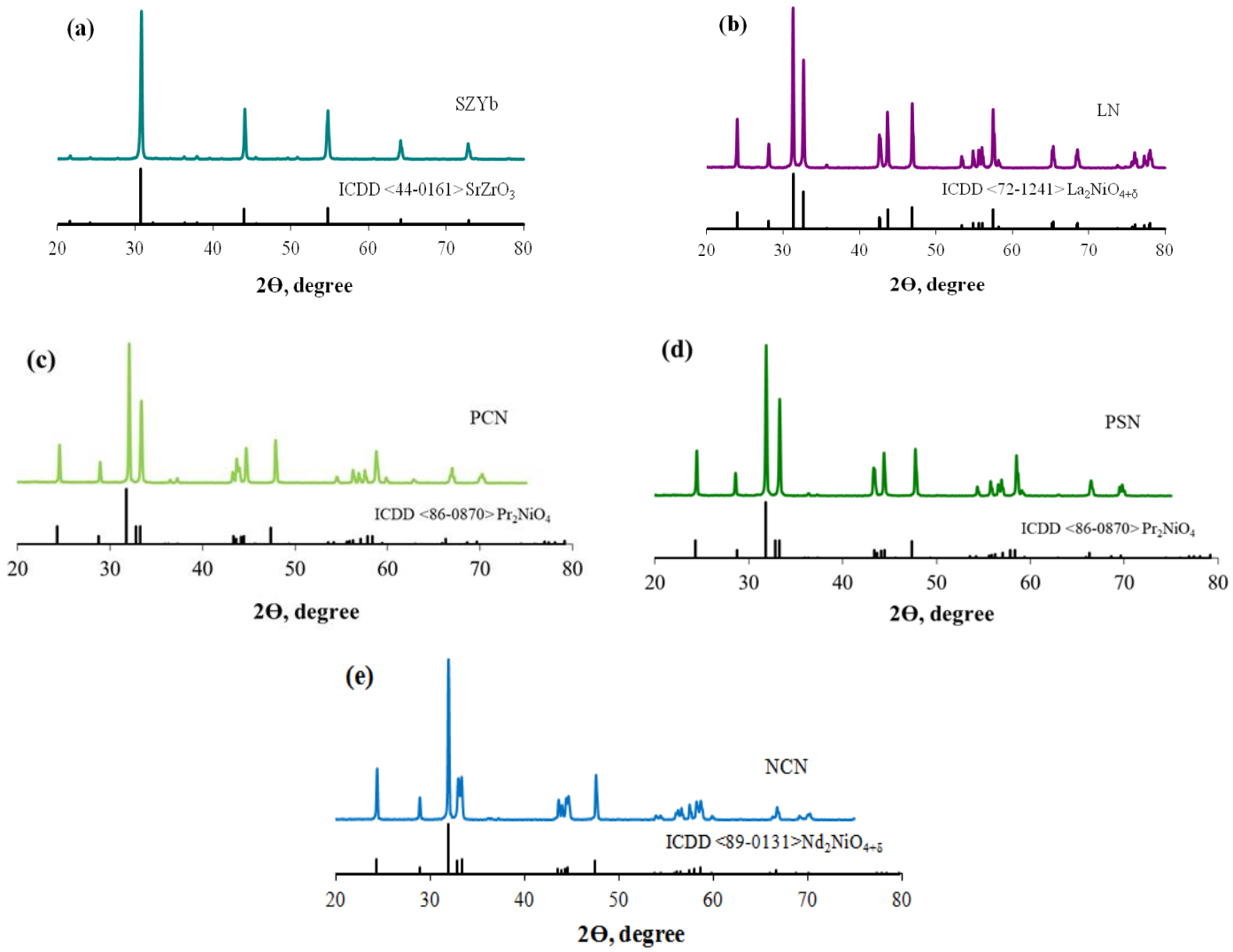

Figure 1 Powder XRD patterns of (a) $Sr_{0.98}Zr_{0.95}Yb_{0.05}O_{3-\delta}$, (b) La_2NiO_4, (c) $Pr_{1.7}Ca_{0.3}NiO_{4+\delta}$, (d) $Pr_{1.7}Sr_{0.3}NiO_{4+\delta}$, (e) $Nd_{1.9}Ca_{0.1}NiO_{4+\delta}$.

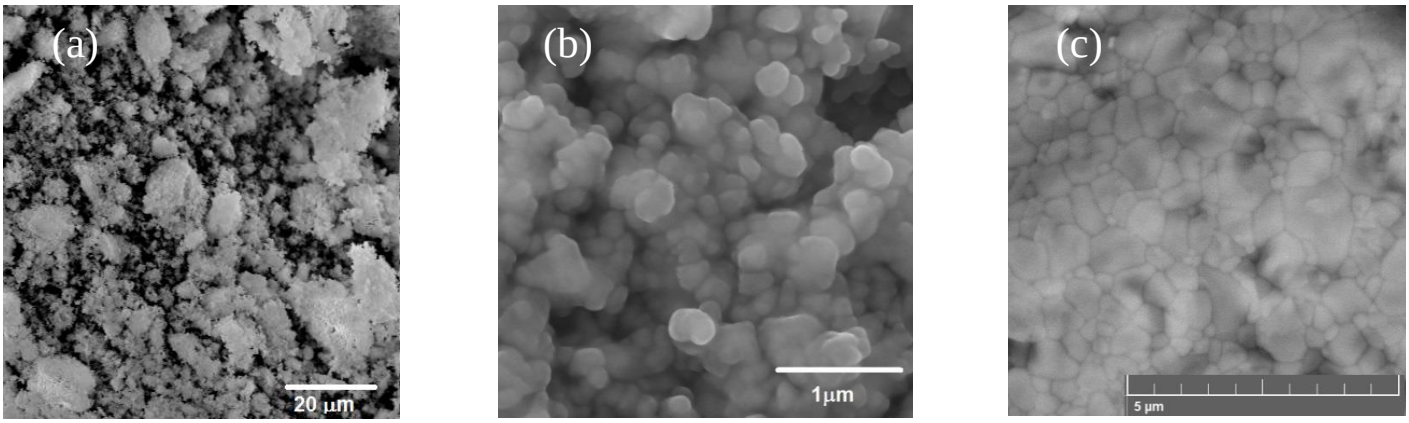

Figure 2 SEM images of SZYb powder synthesized by the solution combustion method (a, b) and surface of sintered SZYb ceramics (c).

LN and NCN exhibit an orthorhombic structure (*Fmmm* space group) with the unit cell parameters of $a = 5.4568(8)$ Å, $b = 5.4647(8)$ Å, $c = 12.6868(13)$ Å, and $a = 5.4568(8)$ Å, $b = 5.4647(8)$ Å, $c = 12.6868(13)$ Å, respectively. PCN and PSN possess a tetragonal structure (*I4/mmm* space group) with $a = b = 3.8044(1)$ Å, $c = 12.3900(2)$ Å, and $a = b = 3.8215(1)$ Å, $c = 12.5011(3)$ Å, respectively. The specific surface area of the $Ln_2NiO_{4+\delta}$ powders was found to be 2.1 (LN), 2.4 (PSN), 2.0 (PCN) and 2.3 (NCN) $m^2 \cdot g^{-1}$. The morphology and particle size of the SZYb powder was evaluated from the SEM images (Figure 2a,b). As can be seen, the powder consists of spherical shaped particles of 100–150 nm aggregated into larger agglomerates. The ceramic sample exhibits a dense structure with the average grain size of ~ 0.5 μm, as was evaluated from the SEM image of the surface of the sintered sample (Figure 2c).

3.2. Study of electrode-electrolyte chemical interaction

To study the chemical stability of the electrolyte and electrode materials in contact with each other at high temperatures, the XRD patterns of the mixtures of SZYb and $Ln_2NiO_{4+\delta}$ powders calcined at temperatures of 1200, 1300 and 1400 °C were analyzed. The diffraction and $Ln_2NiO_{4+\delta}$ powders calcined at temperatures of 1200, 1300 and 1400 °C were analyzed. The diffraction patterns of the mixtures show only the maxima of the original phases, which indicates high chemical stability of all considered nickelates in contact with SZYb perovskite (Figure 3).

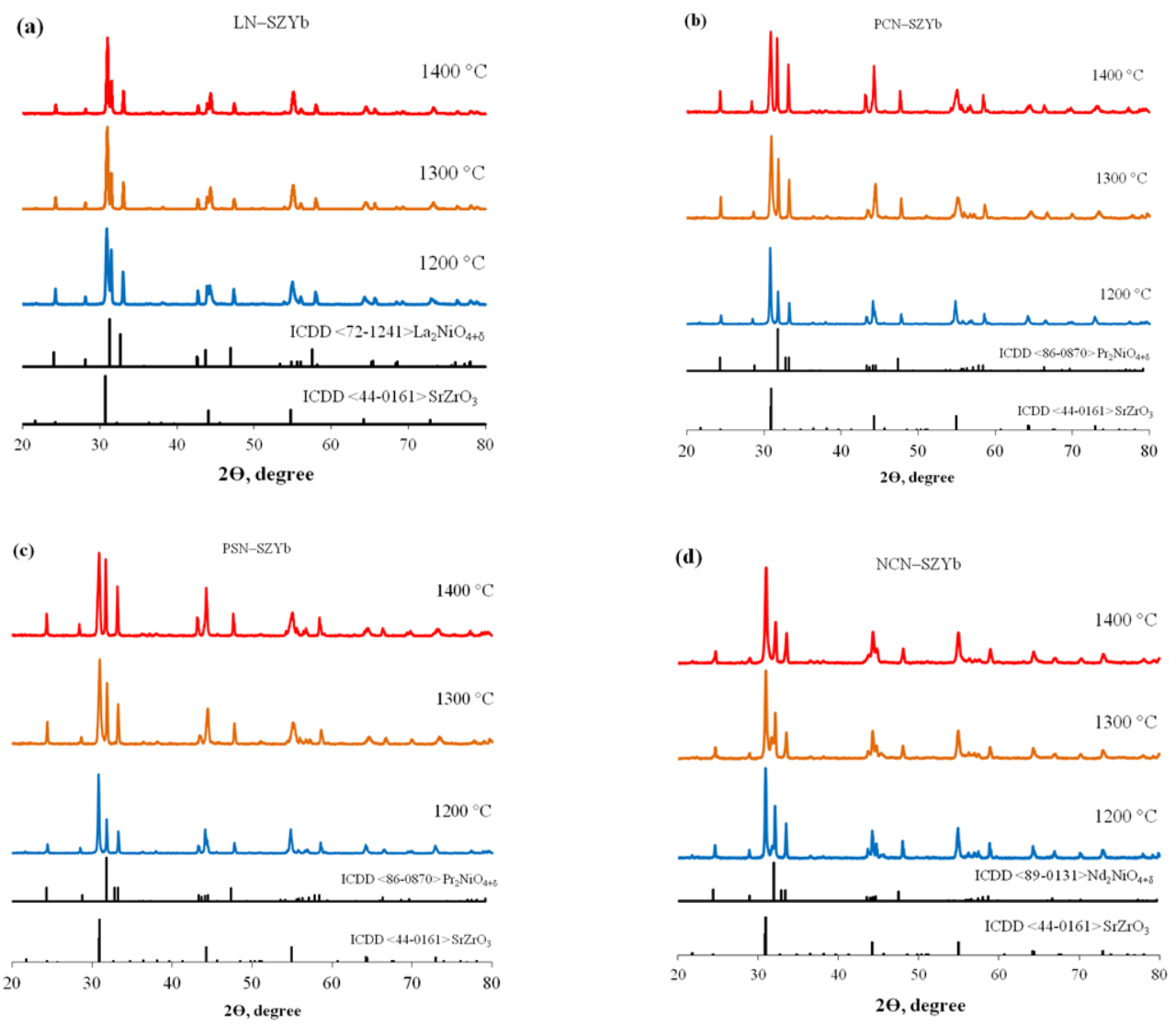

Figure 3 XRD patterns of composites (a) $La_2NiO_{4+\delta}$-SZYb, (b) $Pr_{1.7}Ca_{0.3}NiO_{4+\delta}$-SZYb, (c) $Pr_{1.7}Sr_{0.3}NiO_{4+\delta}$-SZYb, (d) $Nd_{1.9}Ca_{0.1}NiO_{4+\delta}$-SZYb.

3.3. Thermal expansion

The relative expansion of the $Ln_2NiO_{4+\delta}$ samples in the range of 100–900 °C is presented in Figure 4. The LN, PCN and PSN ceramics demonstrate the linear behavior in this range, while the NCN exhibits a small inflection at ~ 560 °C. It can be related to the structural transition *Fmmm* → *I4/mmm* caused by the interstitial oxygen release, which was confirmed by the HT-XRD study in [44]. The tetragonal structure was reliably defined at the temperature of ~ 400 °C; however, the inflection point appears at a higher temperature on the dilatometry curve due to the dynamic regime of measurements. The values of the thermal expansion coefficient (TEC) for the NCN sample were found to be $14.2 \cdot 10^{-6}$ K^{-1} and $16.2 \cdot 10^{-6}$ K^{-1} in the ranges of 100–560 °C and 560–900 °C, respectively. In the LN material, the *Fmmm* → *I4/mmm* transition does not occur up to 700 °C according to the HT-XRD study [45]. That is why there is no inflection point on the dilatometric curve of LN in the studied temperature range. The average TEC values at 100–900 °C were $14.2 \cdot 10^{-6}$ K^{-1} (LN), $14.1 \cdot 10^{-6}$ K^{-1} (PCN), $15.0 \cdot 10^{-6}$ K^{-1} (PSN) and $15.1 \cdot 10^{-6}$ K^{-1} (NCN) (see the insert in Figure 4).

The obtained TEC values of the studied nickelates are consistent with the literature data: TECs of $Ln_2NiO_{4+\delta}$-based materials were reported to vary within $11.5 \cdot 10^{-6}$–$15.5 \cdot 10^{-6}$ K^{-1} in the *RT* to 1000 °C range in air [18]. The thermal expansion coefficient of $SrZr_{0.95}Yb_{0.05}O_{3-\delta}$ was reported to be ~ $10 \cdot 10^{-6}$ K^{-1}, as followed from the experiments on the unit cell parameters variation upon heating from *RT* to 1200 °C [19]. Thus, from the point of view of thermal compatibility, PSN and NCN are less suitable for the SZYb electrolyte compared to LN and PCN.

3.4. Electrical conductivity of $Ln_2NiO_{4+\delta}$-based samples and $Ln_2NiO_{4+\delta}$-SZYb composites

The electrical conductivity of the $Ln_2NiO_{4+\delta}$ materials was reported to be *p*-type, as followed from their positive Seebeck coefficients in a wide range of temperature [46, 47]. In the low temperature range, the conductivity increases with increasing temperature, like in semiconductors. On the basis of the electrical conductivity and oxygen content studies, the hole mobility was found to decrease slightly with increasing temperature, like in metals. In the range of 400–450 °C, the electrical conductivity of $Ln_2NiO_{4+\delta}$ displays a broad maximum, which was supposed to be caused by the transition from semiconducting to pseudo-metallic behavior induced by the loss of interstitial oxygen and related decrease in the concentration of electron holes, and by a decrease in the hole mobility with increasing temperature [46, 47]. As can be seen in Figure 5, the electrical conductivity of the studied nickelates exhibits the similar behavior, which implies the same conduction mechanism. PCN, PSN and NCN demonstrate similar conductivities, while LN has a much lower conductivity.

The electrical conductivity of SZYb perovskite was studied in our recent research [13]; the Arrhenius dependences in the air with different pH_2O values were found to be nearly linear, with the activation energy increasing from 95 to 112 kJ · mol^{-1} (0.99–1.16 eV) with decreasing pH_2O from 3.2 to 0.04 kPa. At high temperatures (above ~ 700 °C), the conductivity does not vary with pH_2O, while at lower temperatures it increases with pH_2O. These features confirm the ionic type of electrical conductivity with the predominance of protonic conductivity in humid air at lower temperatures.

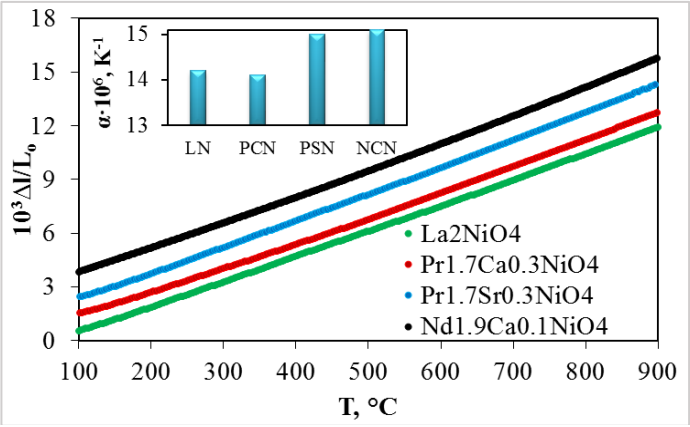

Figure 4 Temperature dependences of the relative expansion of LN, PCN, PSN and NCN samples (shifted along the ordinate axis for better visibility).

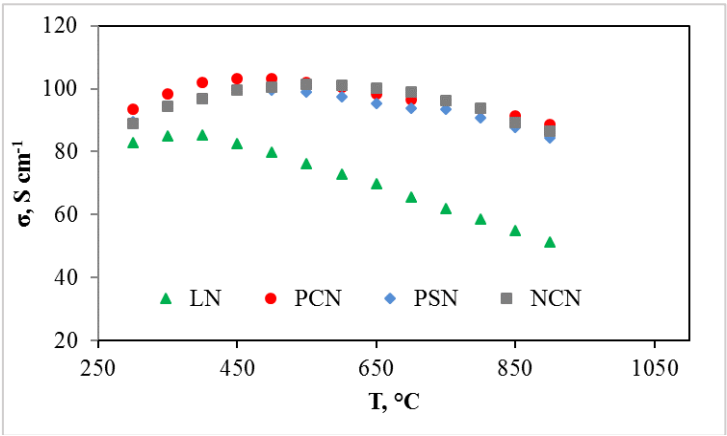

Figure 5 Electrical conductivity of LN, PCN, PSN and NCN *vs* temperature in air.

The temperature dependencies of the electrical conductivity of the $Ln_2NiO_{4+\delta}$-SZYb composite ceramics are presented in Figure 6a. The conductivities increase with temperature displaying a smooth bend at ~ 450 °C, which can be explained by the contribution of $Ln_2NiO_{4+\delta}$-based phase. In contrast to single-phase lanthanide nickelates, the PCN-containing composite ceramic exhibits the highest conductivity, significantly exceeding the conductivity of other composite ceramics, although all samples have a similar density. The regularity in changes in the conductivity of the $Ln_2NiO_{4+\delta}$-SZYb composite ceramics differs from that of single-phase $Ln_2NiO_{4+\delta}$ ceramics (see Figures 5 and 6a). This can be caused by differences in the microstructure of the composite ceramics, in particular, the proximity of TEC values of PCN and SZYb should result in the stronger adhesion of the particles and thus improve the inter-particle contact. The electrical conductivity of composites can also be affected by the formation of impurity phases at the $Ln_2NiO_{4+\delta}$/SZYb interfaces that are indistinguishable by the X-ray method. Based on a comparison of the conductivities of PCN and SZYb samples along with those of the PCN-SZYb composite ceramic presented in Figure 6b, it can be concluded that the conductivity of the composite material is mainly determined by the electron-conducting PCN constituent.

As can be seen from Figure 6c, the conductivity of PCN-SZYb does not change with changes in pH_2O, indicating that humidity does not influence the conductivity of the PCN constituent, whose transport properties largely determine the conductivity of the composite ceramic. Taking into account high conductivity, excellent chemical stability and satisfactory thermal behavior, the PCN-SZYb composite material was selected for the study of electrochemical activity as the oxygen electrode for the SZYb electrolyte.

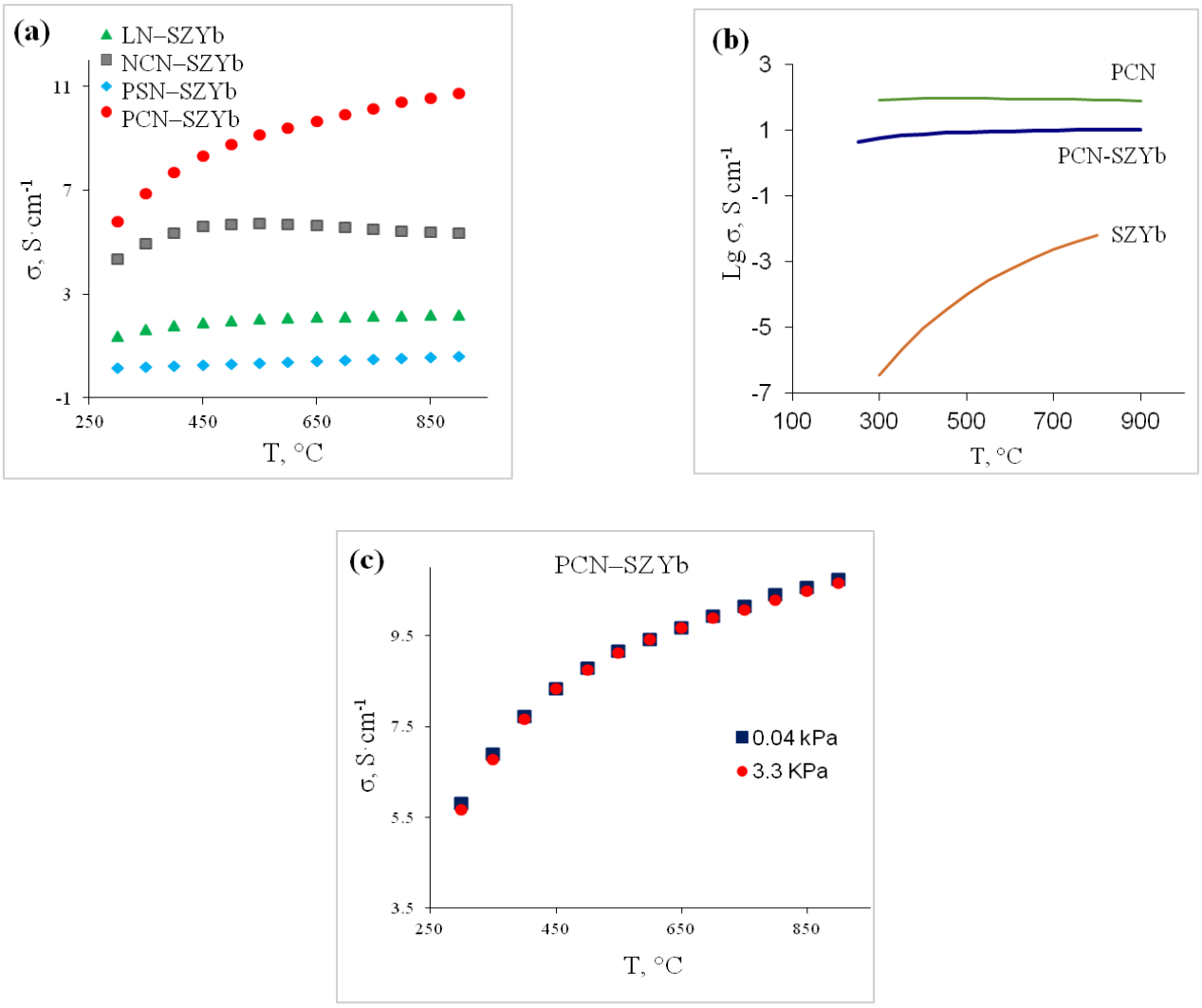

Figure 6 Temperature dependencies of electrical conductivity of (a) $Ln_2NiO_{4+\delta}$-SZYb composites in dry air, (b) PCN, SZYb and PCN-SZYb composite in dry air, (c) PCN-SZYb composite in dry and humid air.

3.5. Electrochemical performance of the PCN-SZYb | SZYb | PCN-SZYb cells

The SEM image of the cross-sectional surface of the button cell PCN-SZYb | SZYb | PCN-SZYb is shown in Figure 7. The thickness of the composite electrode layer is about 15 μm. For the electrochemical measurements, the Pt current collector of the same thickness was applied on the composite electrode surface for a more homogeneous current distribution. As follows from the SEM image, the electrode layer adheres well to the electrolyte and has a porous microstructure, which is required for the fast gas diffusion.

The electrochemical performance of the PCN-SZYb | SZYb | PCN-SZYb cells with pure (Cell 1) and Pr_6O_{11}-treated electrodes (Cells 2 and 3) was investigated by means of impedance spectroscopy and cyclic voltammetry. To illustrate the processing of impedance and current-voltage data, Figure 8 a demonstrates the Nyquist plots of Cell 3 recorded at 550 °C in air with different pH_2Os. As can be seen, each hodograph consists of a high-frequency semicircle intersecting the abscissa axis if extrapolated to higher frequencies, and a part of a low-frequency arc. Taking into account the characteristic capacitance (~ 10^{-9} F) of the high-frequency semicircle, it was attributed to the grain boundaries of SZYb electrolyte; and the segment cut off at high frequencies was ascribed to the resistance of grain interior of the electrolyte. As can be seen from Figure 8a, the resistance of SZYb decreases with pH_2O, confirming the increasing contribution of proton transport.

The low frequency part of hodographs can be attributed to the polarization resistance of the electrodes. Since the capabilities of the device do not allow us to obtain the lowest frequency part of the hodographs, the reliable determination of the total cell resistance, and, therefore, the electrode polarization resistance, from the impedance spectra is difficult. For solving this problem, after recording each hodograph, we measured the current-voltage dependence at low applied voltages. These dependencies were found to be nearly linear (see Figure 8b), which allowed us to determine the total cell resistance from their slopes.

In Figure 8a, the total cell resistances are marked with empty symbols. The polarization resistance was determined as a segment, the left end of which is the intersection of the low-frequency arc with the abscissa axis, and the right end is the total cell resistance calculated from the current-voltage dependence.

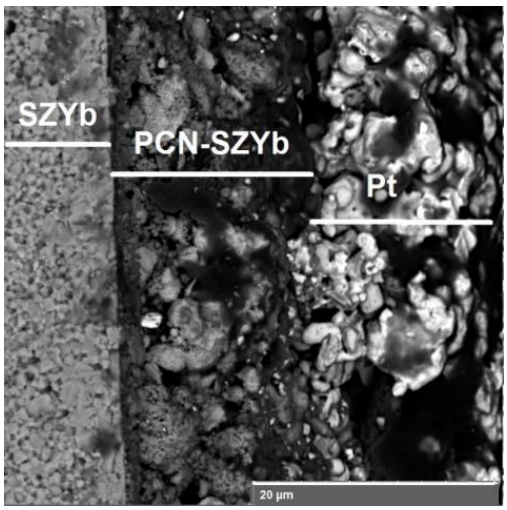

Figure 7 SEM image of the cross-sectional fracture surface of the cell PCN-SZYb | SZYb | PCN-SZYb.

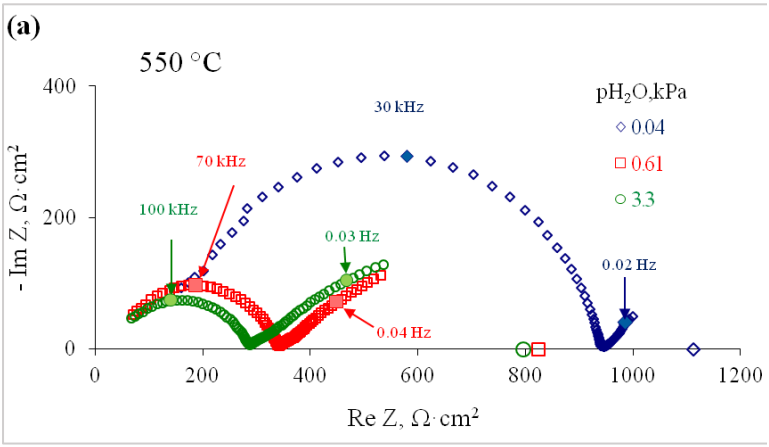

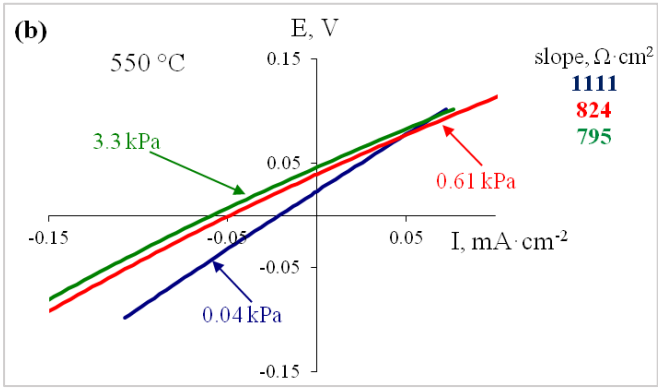

Figure 8 Impedance spectra (a) and current-voltage dependencies (b) of Cell 3 recorded at 550 °C in air with different humidities.

The dependencies of the reciprocal area specific polarization resistance of Cells 1–3 on temperature at pH_2O = 0.61 kPa are summarized in Figure 9. In the high temperature range (500–800 °C), the dependencies are almost linear and display close slopes, which indicates similar values of the apparent activation energy (~ 1.73 eV). A smooth bend is observed at ~ 500 °C, so that the activation energy in the low temperature range decreases to ~ 0.95 eV. This deviation can be caused by the change in the conductivity of PCN component of the electrode (see Figures 5 and 6).

The appearance of proton conduction in SZYb, which is a part of the composite electrode, may also contribute to a decrease in the apparent activation energy with decreasing temperature. The impregnation of the electrodes with the praseodymium nitrate solution results in a decrease in the polarization resistance by about 3 times. Cells 2 and 3 demonstrate almost identical behavior, which indicates that the addition of more than 0.14 mL · cm^{-2} of solution (1.8 mg Pr_6O_{11} cm^{-2}) is not justified.

Thus, the impregnation of the PCN-SZYb electrodes with the praseodymium nitrate solution decreases the polarization resistance. Nevertheless, in the both pristine and Pr_6O_{11}-treated cells, the area specific polarization resistance increases with increasing pH_2O, as can be seen in Figure 10 which displays the temperature dependences of the reciprocal area specific polarization resistance of Cells 1–3 at different values of pH_2O in air. This phenomenon can be explained by a decrease in the hole concentration in the proton-conducting electrolytes in humid air due to the incorporation of water and the related shrinkage of the area where electrochemical reactions occur, as was discussed, for example, in [13, 48]. Besides, adsorption of water molecules may inhibit the electrode surface activity by blocking the electrocatalytic active sites for the redox reactions [49].

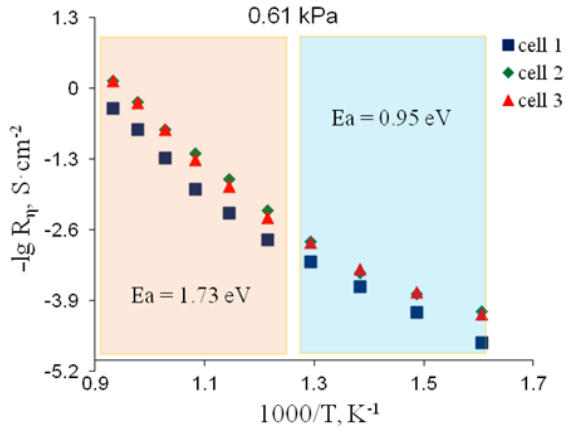

Figure 9 Temperature dependencies of the reciprocal area specific polarization resistance of Cells 1–3 at pH_2O = 0.61 kPa.

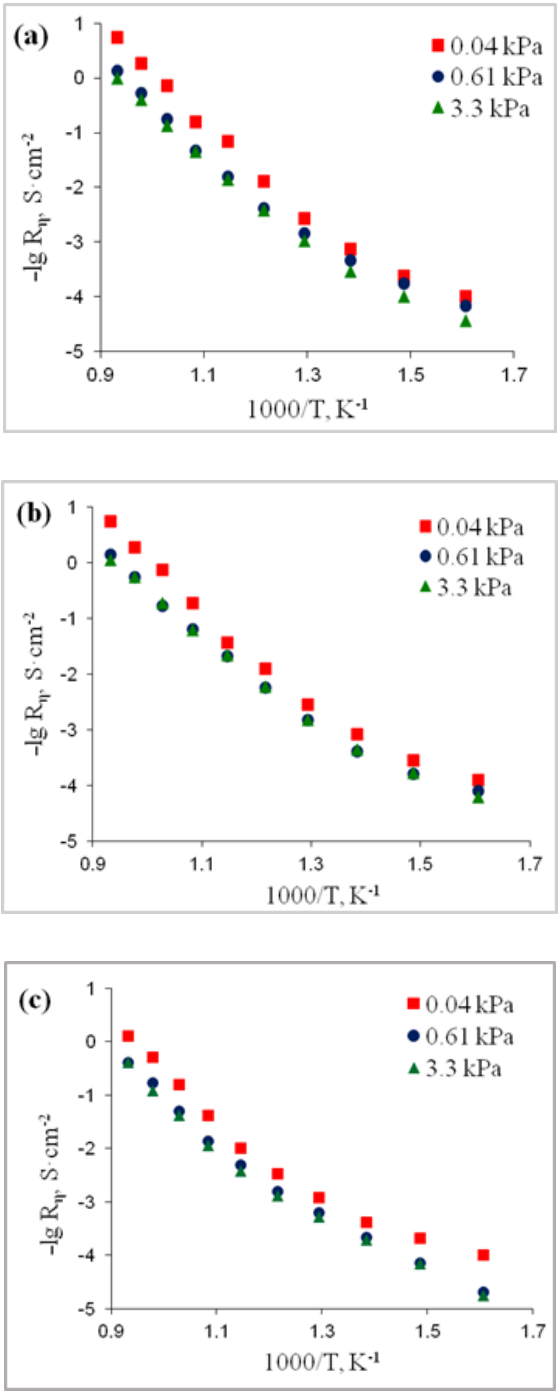

Figure 10 Temperature dependencies of the reciprocal area specific polarization resistance of Cells 1–3 at different values of pH_2O in air: (a) Cell 1, (b) Cell 2, (c) Cell 3.

Figure 11 shows the total, ohmic and polarization area specific resistances of Cell 2 as the functions of humidity at different temperatures. As can be seen, increasing air humidity has the opposite effect on the ohmic and polarization resistances of the cell. The ohmic losses decrease with increasing pH_2O obviously due to the increasing contribution of proton transport in the SZYb electrolyte, while the electrode polarization increases. However, a more intense change in the ohmic

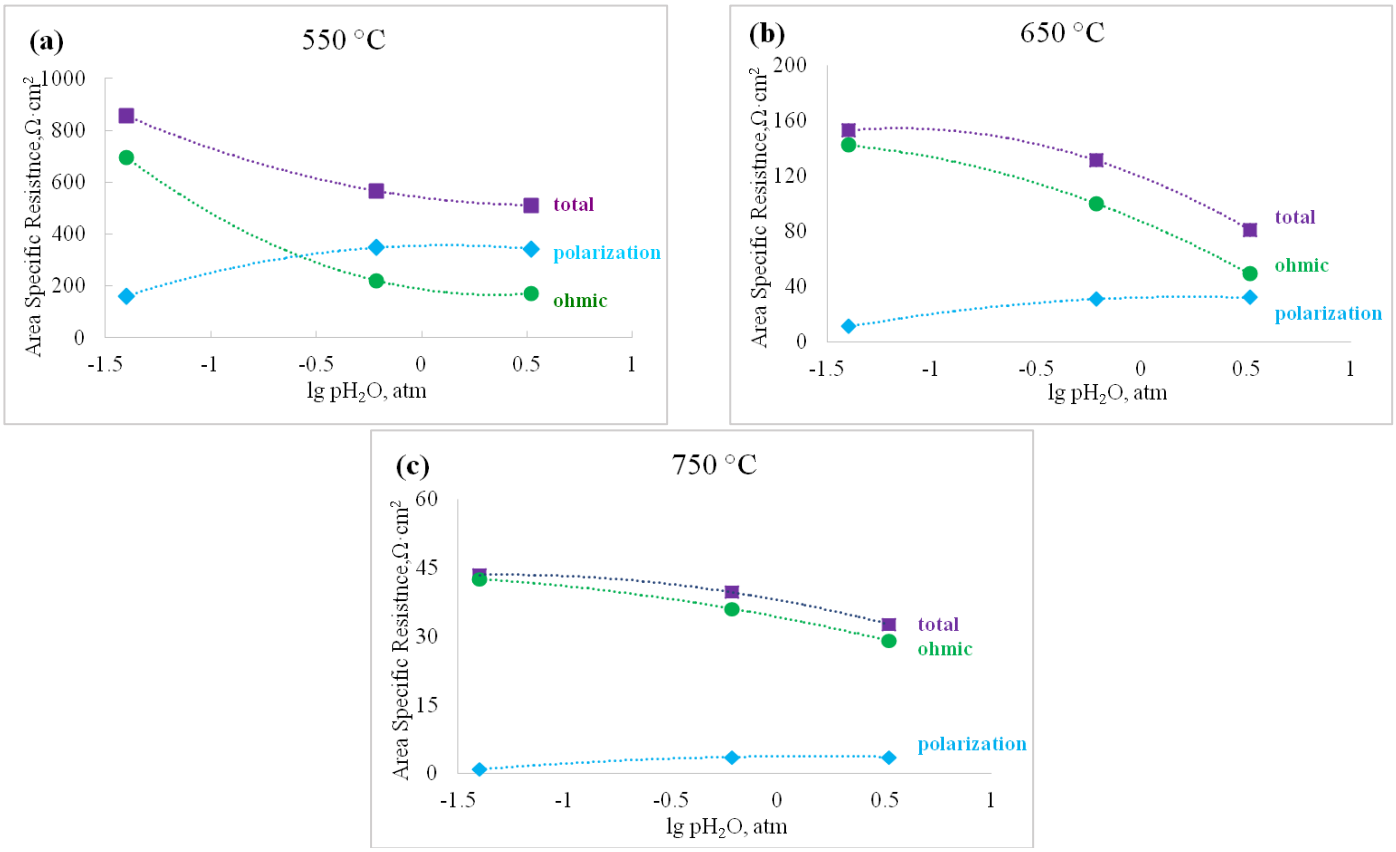

Figure 11 Total, ohmic and polarization area specific resistances of Cell 2 *vs* pH_2O at (a) 550 °C, (b) 650 °C, (c) 750 °C.

contribution compared to the polarization one leads to a decrease in the total resistance with increasing humidity. With increasing temperature, the polarization resistance decreases faster than the resistance of the electrolyte due to a higher activation energy (1.73 eV *vs* 0.99–1.16 eV), as a result, the electrolyte resistance is almost an order of magnitude higher than the polarization resistance at 750 °C. However, the ohmic losses can be significantly diminished by reducing the electrolyte thickness: the area specific ohmic resistance will decrease by almost an order of magnitude if the thickness of a supporting electrolyte is reduced to 150 μm, which is achievable using, for example, tape-casting technology [50].

The obtained results on the polarization resistance of the SZYb electrolyte-supported cells with the composite PCN-SZYb electrodes were compared with the data reported in literature. It should be mentioned that the rate of redox reactions occurring at the triple phase boundary strongly depends on the charge transport properties (the ionic and electronic conductivities, the ionic transference number) of both the electrolyte and electrode materials; therefore, the performance of the cells made of the related materials must be analyzed. The electrochemical cells with the proton-conducting $CaZr_{0.95}Sc_{0.05}O_{3-\delta}$ supporting electrolyte and the composite electrodes containing the $Ln_2NiO_{4+\delta}$-based phase exhibited the area specific polarization resistances in the range of ~ 10–100 Ω · cm² at 700 °C in humid air (pH_2O = 2.5 kPa) [51]. On the other hand, the cells with the Ba(Ce,Zr)O_3-based electrolyte, which possess the higher ionic conductivity, but lower ionic transference numbers than $CaZrO_3$- and $SrZrO_3$-based electrolytes [52–54], and the nickelate-containing composite electrodes were reported to have the polarization resistance of ~ 0.1–1 Ω · cm² (700 °C, ambient air) [55]. The higher values of the polarization resistances obtained in the present research (Cell 2: ~ 10 Ω · cm² at 700 °C, air, pH_2O = 3.3 kPa) than those for PCN-based electrodes in the case of Ba(Ce,Zr)O_3-based electrolytes [55], can be explained by the intrinsic electrolyte properties.

4. Conclusions

The research explored the possibility of using some layered nickelates, namely $La_2NiO_{4+\delta}$ (LN), $Pr_{1.7}Sr_{0.3}NiO_{4+\delta}$ (PSN), $Pr_{1.7}Ca_{0.3}NiO_{4+\delta}$ (PCN), and $Nd_{1.9}Ca_{0.1}NiO_{4+\delta}$ (NCN), as oxygen electrodes for the $Sr_{0.98}Zr_{0.95}Yb_{0.05}O_{3-\delta}$ (SZYb) electrolyte for application in proton-conducting electrochemical cells. Based on the chemical stability, thermal expansion and electrical conductivity studies, the composite material consisting

of PCN and SZYb oxides in a weight ratio of 1 : 1 was selected as the most suitable oxygen electrode. The electrochemical behavior of the SZYb-supported cells with the symmetrical porous PCN-SZYb electrodes supplied with Pt collector was investigated in air with different humidities in the temperature range of 350–800 °C. It was found that the polarization resistance of the cells obeys the Arrhenius law and increases with pH_2O. The impregnation of the porous electrode backbone with the praseodymium nitrate solution enhanced the activity of the electrodes by about 3 times. The electrochemical behavior of the PCN-SZYb electrode in contact with the SZYb electrolyte is consistent with the literature data on the $Ln_2NiO_{4+\delta}$-based electrodes and related proton-conducting electrolytes. The PCN-SZYb composite electrode impregnated with the praseodymium nitrate solution can be used as the oxygen electrode in SZYb-based IT-SOFCs. Further studies can be directed on the modification of microstructure of the composite electrodes and selection of suitable oxide collectors to enhance electrochemical activity and cost efficiency.

Supplementary materials

No supplementary materials are available.

Funding

This research had no external funding.

Acknowledgments

This work was prepared within the framework of the budgetary plans of the Institute of High Temperature Electrochemistry (IHTE) with the facilities of the IHTE Shared Access Centre “Composition of Compounds”.

Author contributions

Anastasia Meshcherskikh: Investigations; Methodology; Data curation; Formal analysis; Visualization.

Adelya Khaliullina: Investigations; Methodology; Data curation; Formal analysis; Visualization.

Elena Pikalova: Formal analysis; Visualization; Writing – Review & Editing.

Liliya Dunyushkina: Conceptualization; Data curation; Formal analysis; Supervision; Writing – Original draft; Writing – Review & Editing.

Conflict of interest

The authors declare no conflict of interest.

Additional information

Anastasia Meshcherskikh, Scopus Author ID: 56784365300;

Adelya Khaliullina, Scopus Author ID: 57206712878;

Elena Pikalova, Scopus Author ID: 16242376500;

Liliya Dunyushkina, Scopus Author ID: 6507914539.

References

1. Xu Q, Guo Z, Xia L, He Q, et al., A comprehensive review of solid oxide fuel cells operating on various promising alternative fuels, Energy Conversion and Management, **253** (2022) 115175. https://doi.org/10.1016/j.enconman.2021.115175

2. Dawood F, Anda M, Shafiullah GM, Hydrogen production for energy: an overview, Int. J. Hydrogen Energy, **45** (2020) 3847–3869. https://doi.org/10.1016/j.ijhydene.2019.12.059

3. Choi S, Davenport TC, Haile SM, Protonic ceramic electrochemical cells for hydrogen production and electricity generation: Exceptional reversibility, stability, and demonstrated faradaic efficiency, Energy Environ. Sci., **12** (2019) 206–215. https://doi.org/10.1039/C8EE02865F

4. Duan C, Huang J, Sullivan N, O’Hayre R, Proton-conducting oxides for energy conversion and storage, Appl. Phys. Rev., **7** (2020) 011314. https://doi.org/10.1063/1.5135319

5. Zhang W, Hu YH, Progress in proton-conducting oxides as electrolytes for low-temperature solid oxide fuel cells: From materials to devices, Energy Sci. Eng., **9** (2021) 984–1011. https://doi.org/10.1002/ese3.886

6. Yajima T, Suzuki H, Yogo T, Iwahara H, Protonic conduction in $SrZrO_3$-based oxides. Solid State Ionics, **51** (1992) 101–107. https://doi.org/10.1016/0167-2738(92)90351-O

7. Zajac W, Rusinek D, Zheng K, Molenda J, Applicability of Gd-doped $BaZrO_3$, $SrZrO_3$, $BaCeO_3$ and $SrCeO_3$ proton conducting perovskites as electrolytes for solid oxide fuel cells, Cent. Eur. J. Chem., **11** (2013) 471–484. https://doi.org/10.2478/s11532-012-0144-9

8. Gharbage B, Marques FMB, Frade JR, Protonic conduction in $Sr_{1-y}(Zr_{1-x}Dy_x)O_{3-d}$ ceramics, J. Eur. Ceram. Soc., **16** (1996) 1149–1156. https://doi.org/10.1016/0955-2219(96)00052-0

9. Higuchi T, Tsukamoto T, Sata N, Hiramoto K, et al., Protonic conduction in the single crystals of $SrZr_{0.95}M_{0.05}O_3$ (M = Y, Sc, Yb, Er), Jpn. J. Appl. Phys., **40** (2001) 4162–4163. https://doi.org/10.1143/JJAP.40.4162

10. Dunyushkina LA, Khaliullina ASh, Meshcherskikh AN, Pankratov AA, et al., Effect of A-site nonstoichiometry on defect chemistry and electrical conductivity of undoped and Y-doped $SrZrO_3$, Materials, **12** (2019) 1258. https://doi.org/10.3390/ma12081258

11. Shkerin SN, Rudakova AV, Bulanin KM, Khaliullina ASh, et al., Raman spectroscopy of $SrZrO_3$ based proton conducting electrolyte: Effect of Y-doping and Sr-nonstoichiometry, Int. J. Hydrogen Energy, **46** (2021) 17007–17018. https://doi.org/10.1016/j.ijhydene.2020.11.236

12. Balakireva VB, Gorelov VP, Dunyushkina LA, Kuzmin AV, Impact of Humidity on Charge Transport in Proton-Conducting Perovskites $AZr_{0.95}Sc_{0.05}O_{3-d}$ (A = Ca, Sr, Ba) Exposed to an Oxidative Atmosphere, Phys. Solid State, **61** (2019) 515–522. https://doi.org/10.1134/S1063783419040048

13. Khaliullina A, Meshcherskikh A, Pankratov A, Dunyushkina L, Effect of Sr deficiency on electrical conductivity of Yb-doped strontium zirconate, Materials, **15** (2022) 4126. https://doi.org/10.3390/ma15124126

14. Khaliullina A, Meshcherskikh A, Dunyushkina L, Effect of cation nonstoichiometry on hydration and charge transport processes in Yb-doped $SrZrO_3$ perovskite-type proton conductor for ceramic electrochemical cells, Processes, **11** (2023) 2939. https://doi.org/10.3390/pr11102939

15. Sadykov VA, Muzykantov VS, Yeremeev NF, PelipenkoVV, et al., Solid Oxide Fuel Cell Cathodes: Importance of Chemical Composition and Morphology, Catalysis for Sustainable Energy, **2(1)** (2015) 57–70. https://doi.org/10.1515/cse-2015-0004

16. Gao Y, Zhang M, Fu M, Hu W, et al., A comprehensive review of recent progresses in cathode materials for proton-conducting SOFCs, Energy Reviews, **2(3)** (2023) 100038, https://doi.org/10.1016/j.enrev.2023.100038

17. Song J, Ning D, Boukamp B, Bassat JM, et al., Structure, electrical conductivity and oxygen transport properties of Ruddlesden–Popper phases $Ln_{n+1}Ni_nO_{3n+1}$ (Ln = La, Pr and Nd; n = 1, 2 and 3), J. Mater. Chem. A, **8** (2020) 22206. https://doi.org/10.1039/d0ta06731h

18. Morales-Zapata MA, Larrea A, Laguna-Bercero MA, Lanthanide nickelates for their application on Solid Oxide Cells, Electrochimica Acta, **444** (2023) 141970. https://doi.org/10.1016/j.electacta.2023.141970

19. Osaka T, Numako C, Koto K, Local structure and thermal study of ytterbium-doped $SrZrO_3$, Materials Research Bulletin, **34** (1999) 11–24. https://doi.org/10.1016/S0025-5408(98)00209-8

20. Greenblatt M, Ruddlesden-Popper properties $Ln_{n+1}Ni_nO_{3n+1}$ nickelates: structure and properties, Curr. Opin. Solid State Mater. Sci., **2** (1997) 174–183. https://doi.org/10.1016/s1359-0286(97)80062-9

21. Kharton VV, Viskup AP, Naumovich EN, Marques FMB, Oxygen ion transport in La_2NiO_4-based ceramics, J. Mater., **9** (1999) 2623–2629. https://doi.org/10.1039/A903276B

22. Skinner SJ, Kilner JA, Oxygen diffusion and surface exchange in $La_{2-x}Sr_xNiO_{4+\delta}$, Solid State Ionics **135** (2000) 709–712. https://doi.org/10.1016/S0167-2738(00)00388-X

23. Bassat JM, Odier P, Villesuzanne A, Marin C, et al., Anisotropic ionic transport properties in $La_2NiO_{4+\delta}$ single crystals, Solid State Ionics, **167** (2004) 341–347. https://doi.org/10.1016/j.ssi.2003.12.012

24. Lee Y, Kim H, Electrochemical performance of $La_2NiO_{4+\delta}$ cathode for intermediate-temperature solid oxide fuel cells, Ceram. Int., **41** (2015) 5984–5991. https://doi.org/10.1016/j.ceramint.2015.01.037

25. Nicollet C, Flura A, Vibhu V, Rougieret A, et al., $La_2NiO_{4+\delta}$ infiltrated into gadolinium doped ceria as novel solid oxide fuel cell cathodes: electrochemical performance and impedance modeling, J. Power Sources, **294** (2015) 473–482. https://doi.org/10.1016/j.jpowsour.2015.06.077

26. Woolley RJ, Skinner SJ, Functionally graded composite $La_2NiO_{4+\delta}$ and $La_4Ni_3O_{10-\delta}$ solid oxide fuel cell cathodes, Solid State Ionics, **255** (2014) 1–5. https://doi.org/10.1016/j.ssi.2013.11.041

27. Zhao K, Wang Y-P, Chen M, Xu Q, et al., Electrochemical evaluation of $La_2NiO_{4+\delta}$ as a cathode material for intermediate temperature solid oxide fuel cells, Int. J. Hydrog. Energy, **39** (2014) 7120–7130. https://doi.org/10.1016/j.ijhydene.2014.02.106

28. Kolchugin AA, Pikalova EY, Bogdanovich NM, Bronin DI, et al., Structural, electrical and electrochemical properties of calcium-doped lanthanum nickelate, Solid State Ionics, **288** (2016) 48–53. https://doi.org/10.1016/j.ssi.2016.01.035

29. Tarutin A, Lyagaeva J, Farlenkov A, Plaksin S, et al., Reversible Protonic Ceramic Cell with Symmetrically Designed $Pr_2NiO_{4+\delta}$-Based Electrodes: Fabrication and Electrochemical Features, Materials, **12(1)** (2019) 118. https://doi.org/10.3390/ma12010118

30. Hyegsoon A, Dongwook S, Ho-Il J, $Pr_2NiO_{4+\delta}$ for Cathode in Protonic Ceramic Fuel Cells, J. Korean Ceram. Soc., **55(4)** (2018) 358–363. https://doi.org/10.4191/kcers.2018.55.4.06

31. Grimaud A, Mauvy F, Bassat JM, Fourcade S, et al., Hydration and transport properties of the $Pr_{2-x}Sr_xNiO_{4+\delta}$ compounds as H^+-SOFC cathodes, J. Mater. Chem., **22** (2012) 16017–16025 https://doi.org/10.1039/C2JM31812A

32. Pikalova E, Zhulanova T, Ivanova A, Tarutin A, et al., Optimized $Pr_{1.6}Ca_{0.4}Ni_{1-y}Cu_yO_{4+\delta}$ phases as promising electrode materials for CeO_2- and $BaCe(Zr)O_3$-based electrochemical cells, Ceramics International, **50(20) Part C** (2024) 40476–40491. https://doi.org/10.1016/j.ceramint.2024.06.048

33. Yang X, Xu X, Wu S, Yu S, et al., Enhancing the performance of traditional $La_2NiO_{4+\delta}$ cathode for proton-conducting solid oxide fuel cells with Zn-doping, Ceramics International, **48(14)** (2022) 19626–19632. https://doi.org/10.1016/j.ceramint.2022.03.098

34 Pikalova EY, Kolchugin AA, The Influence of the Substituting Element (M = Ca, Sr, Ba) in $La_{1.7}M_{0.3}NiO_{4+\delta}$ on the Electrochemical Performance of the Composite Electrodes, Eurasian Chemico-Technological Journal, **18(1)** (2016) 3–11. https://doi.org/10.18321/ectj386

35. Antonova EP, Kolchugin AA, Pikalova EY, Medvedev DA, et al., Development of electrochemically active electrodes for $BaCe_{0.89}Gd_{0.1}Cu_{0.01}O_{3-\delta}$ proton conducting electrolyte, Solid State Ionics, **306** (2017) 55–61. https://doi.org/10.1016/j.ssi.2017.02.001

36. Danilov N, Lyagaeva J, Vdovin G, Pikalova E, et al., Electricity/hydrogen conversion by the means of a protonic ceramic electrolysis cell with $Nd_2NiO_{4+\delta}$-based oxygen electrode, Energy Conversion and Management, **172** (2018) 129–137. https://doi.org/10.1016/j.enconman.2018.07.014

37. Gilev AR, Sukhanov KS, Kiselev EA, Sobol ME, et al., Increasing thermodynamic stability and electrochemical performance of IT-SOFC cathodes based on Ln_2MO_4 (Ln = La, Pr; M = Ni, Cu), Ceramics International, **50(20) Part C** (2024) 40453–40463. https://doi.org/10.1016/j.ceramint.2024.04.176

38. Solis C, Navarrete L, Serra JM, Study of Pr and Pr and Co doped $La_2NiO_{4+\delta}$ as cathodes for $La_{5.5}WO_{11.25-\delta}$ based protonic conducting fuel cells, Journal of Power Sources, **240** (2013) 691–697. https://doi.org/10.1016/j.jpowsour.2013.05.055

39. Pikalova EYu, Bogdanovich NM, Kuz'min AV, Composite electrodes for proton conducting electrolyte of $CaZr_{0.95}Sc_{0.05}O_{3-\delta}$, Russian Journal of Electrochemistry, **53(7)** (2017) 846–855. https://doi.org/10.1134/S1023193517070096

40. Antonova EP, Stroeva AY, Tropin ES, Electrode performance of $La_2NiO_{4+\delta}$ cathodes in contact with $La_{0.9}Sr_{0.1}ScO_{3-\delta}$ proton-conducting oxide, J. Solid State Electrochem., **24** (2020) 1447–1451. https://doi.org/10.1007/s10008-020-04535-z

41. Oh S, Kim H, Jeong I, Kim D, et al., Recent progress in oxygen electrodes for protonic ceramic electrochemical cells, J. Korean Ceram. Soc., **61** (2024) 224–249. https://doi.org/10.1007/s43207-023-00360-y

42. Vshivkova AI, Gorelov VP, Kuzmin AV, Plaksin SV, et al., Preparation and physicochemical properties of praseodymium oxide films and ceramics, Inorganic Materials, **51(11)** 2015 1168–1176. https://doi.org/10.1134/S0020168515100179

43. Vashook V, Girdauskaite E, Zosel J, Wen TL, et al., Oxygen non-stoichiometry and electrical conductivity of $Pr_{2-x}Sr_xNiO_{4\pm\delta}$ with x=0–0.5, Solid State Ionics, **177(13–14)** (2006) 1163–1171. https://doi.org/10.1016/j.ssi.2006.05.018

44. Pikalova E, Kolchugin A, Filonova E, Bogdanovich N, et al., Validation of calcium-doped neodymium nickelates as SOFC air electrode materials, Solid State Ionics, **319** (2018) 130–140. https://doi.org/10.1016/j.ssi.2018.02.008

45. Pikalova E, Sadykov V, Sadovskaya E, Yeremeev N, et al., Correlation between Structural and Transport Properties of Ca-Doped La Nickelates and Their Electrochemical Performance, Crystals, **11(3)** (2021) 297. https://doi.org/10.3390/cryst11030297

46. Nakamura T, Yashiro K, Sato K, Mizusaki J, Electrical conductivity, Seebeck coefficient, and defect structure of oxygen nonstoichiometric $Nd_{2-x}Sr_xNiO_{4+\delta}$, Materials Chemistry and Physics, **122(1)** (2010) 250–258. https://doi.org/10.1016/j.matchemphys.2010.02.044

47. Nakamura T, Yashiro K, Sato K, Mizusaki J, Electronic state of oxygen nonstoichiometric $La_{2-x}Sr_xNiO_{4+\delta}$ at high temperatures, Phys. Chem. Chem. Phys., **11** (2009) 3055–3062. https://doi.org/10.1039/B823364K

48. Taherparvar H, Kilner JA, Baker RT, Sahibzada M, Effect of Humidification at Anode and Cathode in Proton-Conducting SOFCs, Solid State Ionics, **162–163** (2003) 297–303. https://doi.org/10.1016/S0167-2738(03)00222-4

49. Dong K, Miao L, Hou J, Liu W, A novel inhibiting water adsorption strategy to enhance the cathode electrocatalytic ability, Journal of Alloys and Compounds, **876** (2021) 160205. https://doi.org/10.1016/j.jallcom.2021.160205

50. Kwon Y, Han Y, Fabrication of electrolyte-supported solid oxide fuel cells using a tape casting process, Journal of the Ceramic Society of Japan, **128(6)** (2020) 310–316. http://doi.org/10.2109/jcersj2.20006

51. Pikalova EYu, Bogdanovich NM, Kuzmin AV, Composite electrodes for proton conducting electrolyte of $CaZr_{0.95}Sc_{0.05}O_{3-\delta}$, Russian Journal of Electrochemistry, **53(7)** (2017) 752–760. http://doi.org/10.1134/S1023193517070096

52. Gorelov VP, Balakireva VB, Kuzmin AV, Charge transfer and defect structure in $BaCeO_3$, Russ. J. Inorg. Chem., **63(7)** (2018) 930–937. https://doi.org/10.1134/S0036023618070070

53. Dippon M, Babiniec SM, Ding H, Ricote S, et al., Exploring electronic conduction through $BaCe_xZr_{0.9-x}Y_{0.1}O_{3-\delta}$ proton-conducting ceramics, Solid State Ionics, **286** (2016) 117–121. https://doi.org/10.1016/j.ssi.2016.01.029

54. Kosacki I, Tuller HL, Mixed conductivity in $SrCe_{0.95}Yb_{0.05}O_3$ protonic conductors, Solid State Ionics, **80** (1995) 223–229. https://doi.org/10.1016/0167-2738(95)00142-S

55. Antonova EP, Kolchugin AA, Pikalova EYu, Medvedev DA, et al., Development of electrochemically active electrodes for $BaCe_{0.89}Gd_{0.1}Cu_{0.01}O_{3-\delta}$ proton conducting electrolyte, Solid State Ionics, **306** (2017) 55–61. http://dx.doi.org/10.1016/j.ssi.2017.02.001